DNA Poised for Release in Bacteriophage ø29

Jinghua Tang[1], **Norman Olson**[1], **Paul J. Jardine**[2], **Shelley Grimes**[2], **Dwight L. Anderson**[2,3*], and **Timothy S. Baker**[1,4*]

[1]*Department of Chemistry and Biochemistry, University of California-San Diego, La Jolla, CA 92093*

[2]*Department of Diagnostic and Biological Sciences, Institute for Molecular Virology, University of Minnesota, Minneapolis, MN 55455*

[3]*Department of Microbiology, University of Minnesota, Minneapolis, MN 55455*

[4]*Department of Molecular Biology, University of California-San Diego, La Jolla, CA 92093*

SUMMARY

We present here the first asymmetric, three-dimensional reconstruction of a tailed dsDNA virus, the mature bacteriophage φ29, at sub-nanometer resolution. This structure reveals the rich detail of the asymmetric interactions and conformational dynamics of the φ29 protein and DNA components, and provides novel insight into the mechanics of virus assembly. For example, the dodecameric head-tail connector protein undergoes significant rearrangement upon assembly into the virion. Specific interactions occur between the tightly packed dsDNA and the proteins of the head and tail. Of particular interest and novelty, a ~60Å diameter toroid of dsDNA was observed in the connector-lower collar cavity. The extreme deformation that occurs over a small stretch of DNA is likely a consequence of the high pressure of the packaged genome. This toroid structure may help retain the DNA inside the capsid prior to its injection into the bacterial host.

Keywords

bacteriophage ø29; 3D asymmetric reconstruction; sub-nanometer resolution; electron cryo-microscopy; DNA toroid; DNA packaging

---

INTRODUCTION

Double-stranded DNA (dsDNA) bacteriophages are remarkably efficient, genome-delivery machines. They have long served as model systems for investigating fundamental principles of virus structure and macromolecular assembly (Johnson and Chiu, 2007). Electron cryo-microscopy (cryoEM) and three-dimensional (3D) image reconstruction provide a powerful means to study the structure, complexity and dynamics of a wide range of macromolecular complexes (Jiang and Ludtke, 2005). Additionally, these methods complement atomic-resolution techniques, such as X-ray crystallography, especially when crystals of an entire, functional complex are lacking. When atomic models of components or sub-assemblies are accessible, they can be fitted into reconstructed density maps to produce informative pseudo-atomic models (Mitra and Frank, 2006). Advances in cryoEM and 3D image processing yielded

*Corresponding authors (tsb@ucsd.edu, dlander@umn.edu).

the first sub-nanometer structure determinations of highly symmetric (icosahedral) viruses (including hepatitis (Bottcher et al., 1997; Conway et al., 1997) and papilloma (Trus et al., 1997)), providing significant biological insights that could not have been gleaned from lower resolution reconstructions (Baker et al., 1999).

Recently, a number of asymmetric viruses, including the tailed dsDNA bacteriophages T7, ε15, P22 and ø29, have been characterized using single-particle, cryo-reconstruction methods (Agirrezabala et al., 2005; Chang et al., 2006; Jiang et al., 2006; Lander et al., 2006; Xiang et al., 2006). These phages are asymmetric structures because they exhibit symmetry mismatches between head (five-fold) and tail (six-fold) components. Studies of the tailed phages yielded structures at ~17Å resolution, which is insufficient to distinguish secondary structural features in proteins and DNA. This contrasts with the sub-nanometer resolution that is often now achieved with highly symmetric icosahedral particles (e.g. Jäälinoja et al., 2007; Morais et al., 2005; Zhang et al., 2005; Zhou et al., 2001). Limitations in particle homogeneity and stability, the need for large numbers of images, and barriers in computational resources and algorithms, have collectively hindered attempts to achieve higher resolution with large, asymmetric structures like these phages.

The *Bacillus subtilis* bacteriophage ø29, a tractable machine of considerable complexity, is well suited for unraveling the mechanisms of viral assembly and infection because of the richness and depth of information on ø29 morphogenesis, the nearly complete inventory of gene products encoded by the 19.3kbp dsDNA, and the extensive physiological study of gene functions (Anderson and Reilly, 1993; Grimes et al., 2002; Meijer et al., 2001; Peterson et al., 2001). Moreover, determination of the structure of ø29 is well advanced (Morais et al., 2005; Morais et al., 2003; Morais et al., 2001; Simpson et al., 2000; Tao et al., 1998; Xiang et al., 2006), as is study of its dynamic assembly mechanisms using integrated genetic, biochemical, and biophysical approaches (Anderson and Reilly, 1993; Chemla et al., 2005; Grimes et al., 2002; Meijer et al., 2001; Smith et al., 2001). Briefly, the mature, fiberless ø29 virus particle has a prolate head and a small, non-contractile tail, containing 235 and about 80 protein molecules, respectively. The prolate head shell is comprised of gene product 8 (gp8) and encapsidates the linear, dsDNA genome, which has a copy of the terminal protein, gp3, covalently bound to each 5' end (Meijer et al., 2001). The head-tail connector, a dodecamer of gp10, is embedded within a unique five-fold vertex of the head (Tao et al., 1998). The connector serves as the site of assembly of the transient DNA packaging motor that translocates the dsDNA genome into a precursor head shell, or prohead. Compacting the DNA to near crystalline density requires a force generating capacity exceeding 100 pN (Rickgauer et al., 2008). After packaging, the ATPase and prohead RNA components of the packaging motor are displaced by assembly of the lower collar/tail tube (gp11), followed in sequence by the tail knob (gp9) and twelve appendages (gp12*) (Hagen et al., 1976).

In our quest to detail molecular conformational changes that regulate ø29 assembly and the propulsive events during infection and DNA injection, we have employed asymmetric cryoEM 3D reconstruction to examine the secondary, tertiary, and quaternary structures of all phage components. Concurrently, the fitting of atomic models derived from X-ray crystal structures into these reconstructions continues to provide a complementary approach to vigorously explore the ø29 system (Morais et al., 2005; Morais et al., 2003; Simpson et al., 2000; Xiang et al., 2006). Here we report asymmetric 3D reconstructions of full- and empty-fiberless particles of bacteriophage ø29 at resolutions finer than 10 Å. Details of protein subunit secondary structures, DNA packing and conformation, symmetry mismatches, and the response of DNA to high compression force in the confines of the tail are revealed for the first time. Among the many insights to be gleaned from the new structures, here we focus primarily on the structure of the DNA and demonstrate that a short stretch of it bends sharply into a toroid inside the phage tail.

RESULTS AND DISCUSSION

3D Reconstructions of the Virion and Empty Particle

Low dose images of vitrified samples were used to compute 3D reconstructions of fiberless ø29 virions and empty particles (Fig.1) at resolutions calculated to be 7.8 and 9.3Å, respectively (see Methods). At these resolutions it is possible to assign structural components of the phage, reveal how they interact, and visualize features of secondary structure. In both reconstructions, tubular density features, ascribed to α-helices, were resolved in all 235 copies of gp8 in the prolate head and in all twelve copies of gp10 in the connector (see below). The stability and uniformity of the virion and empty particles required to permit reconstruction at this resolution are quite remarkable. The stoichiometrically distinct head, connector, and tail components, despite their asymmetric distribution, must be in near identical register in all particles.

Similar analysis of stable, asymmetric structures of the ribosome at sub-nanometer resolutions by cryoTEM has greatly expanded our understanding of its functions (Allen and Frank, 2007; Berk and Cate, 2007). As a point of reference, it is noteworthy that the ø29 particles detailed here are more massive by an order of magnitude than the ribosome. Unlike the ribosome, ø29 has fewer unique components, but all (except DNA-gp3) are present in multiple copies as symmetric or quasi-symmetric oligomers whose different stoichiometries lead to symmetry-mismatched interactions believed to impart important functional properties (Hendrix, 1978; Johnson and Chiu, 2007).

The 235 copies of gp8 in the ø29 capsid are arranged in a Q=5 lattice (Aebi et al., 1974; and Fig. 1A) similar to that seen in earlier ø29 reconstructions (Morais et al., 2005; Tao et al., 1998; Xiang et al., 2006). The core of each gp8 subunit, as first revealed in symmetrized reconstructions of isometric variants of the ø29 capsid (Morais et al., 2005), has a structure that resembles the HK97 fold (Wikoff et al., 2000), seemingly common to all tailed, dsDNA phage capsids (Baker et al., 2005). The exterior domain of gp8, which is reported to be analogous to the bacterial immunoglobulin-like BIG2 domain (Morais et al., 2005), forms a prominent feature on the exterior surface of the head (Fig.1A). The twelve-fold tail is attached to the head at a five-fold vertex, where the symmetry mismatch between head and tail is accommodated.

The tail is attached to the head via the dodecameric head-tail connector (Fig. 1 and Fig. 2). The wide end of connector, with its twelve copies of gp10, is embedded among five gp8 hexamers in the head shell. The lower collar/tail tube, comprised of twelve copies of gp11(Carrascosa et al., 1983), are attached to the narrow end of the connector. The tube and gp9 knob at the end of the tail, display smooth, cylindrical morphologies and no recognizable substructures, perhaps indicating that subunits in these regions are packed tightly and contain little, if any, surface protrusions. Twelve appendages that function in viral adsorption, each shown to be a trimer of gp12* (a gp12 cleavage product) (Xiang et al., 2006), contact the interface between gp10 and gp11 via twelve narrow, connecting arms.

Appendages adopt up or down orientations that correlate with the location of each appendage relative to the five-fold symmetry of the head. A thin, longitudinal cross-section from the virion reconstruction (Fig. 2A) captures one appendage in the up (at left side) and another in the down (right side) orientation. A similar pattern of appendage orientations was observed in asymmetric reconstructions of fibered ϕ29 phage and was suggested to be a consequence of interaction of gp12* with the accessory gp8.5 head fibers (Xiang et al., 2006). However, this is not the case here, since the particles we imaged are a fiberless variant. Instead, our density maps show that the connecting arms of gp12* contact the gp8 head shell, thereby suggesting that gp12* conformation is dictated by symmetry mismatched interactions with the shell. Detailed analyses of gp8–gp12* interactions and those between other symmetry-mismatched

subunit pairs such as gp8–gp10, are revealing additional insights about φ29 and are part of ongoing studies (Tang et al., in preparation).

Conformation of the Connector *in Situ* Differs from that in Crystals

Density corresponding to the gp10 dodecamer in the virion (Fig. 3A) and empty particle (data not shown) reconstructions display a large number of tube-like features which are aligned at about a 30° angle to the long axis of the particles. These tubes of density correspond to the α-helices of the connector revealed by high resolution X-ray crystallography (Guasch et al., 2002;Simpson et al., 2000) (Fig. 3B), seen here for the first time in situ. However, conspicuous differences between φ29 connectors in crystals and connectors in virions, as well as empty particles, reveal that the connector is remodeled by its environment in the phage.

As observed in the crystals of the dodecamer (Guasch et al., 2002; Simpson et al., 2000) each gp10 subunit consists of three primary domains (Fig. 3B): an αβ-rich top domain at the wide end of the connector; an α-rich central domain; and an αβ bottom domain, which resembles a "paper clip". The atomic model of the entire gp10 dodecamer, treated as one rigid body, clearly did not fit into the cryoEM density maps (correlation coefficient = 0.55). The top and central domains of all gp10 subunits, when tilted by about 10° towards the connector axis (Fig. 3C), did fit the density nicely (Fig. 3A), as evidenced by a correlation coefficient of 0.70. These fits were aided by the presence and arrangement of several prominent helices. Conversely, the bottom domain could not be fit satisfactorily as a rigid body into the remaining connector density. This density lies much further from the connector axis than does the bottom domain in the crystal structure, and features within this region are not yet well enough resolved to determine if any 'clip' structure is retained. Therefore, the bottom domain likely undergoes significant rearrangement in phage particles. Changes in the angle of the connector core subunit and the remodeling of the 'clip' are presumably induced by interactions made with DNA, gp8, gp11, and gp12*, none of which are present in connector crystals. In empty particles the bottom domain also loses its 'clip' conformation and is folded back, but to a lesser extent as seen in virions (data not shown). With just three snap shots of the connector (one at near atomic resolution in crystals and two at sub-nanometer resolution *in situ*), it is impossible to accurately define, in precise detail, the sequence of changes in connector that accompany various stages of virus assembly. Detailed analysis of these events will require additional structural studies of assembly intermediates at comparable resolutions.

DNA Path from Head to Tail

Comparison of cutaway views of virions and empty particles emphasizes that the primary difference between them is the presence of DNA-gp3 inside the virion (Fig. 1B,C). DNA is densely packed in the virion head, and extends into the tail tube after passing through the connector and lower collar. The bulk DNA inside the prolate head appears to be organized in a series of layers, four of which are clearly evident inside the virion (Fig. 4A). A radial density profile, computed from a planar section perpendicular to the phage axis in the virion 3D map (data not shown), reveals about eight total layers, with a 23Å spacing that is consistent with previous measurements (Subirana et al., 1979). The layered nature of the bulk ø29 DNA is a common feature observed in all previous reconstructions of asymmetric phages (Agirrezabala et al., 2005; Chang et al., 2006; Jiang et al., 2006; Lander et al., 2006) including ø29 (Comolli et al., 2007; Xiang et al., 2006) and has been predicted on the basis of modeling studies (Petrov and Harvey, 2007; Petrov et al., 2007). Unlike previous reconstructions, the sub-nanometer ø29 virion reconstruction reveals for the first time an extensive network of protein-DNA interactions between the DNA and capsid shell (Fig 4B). These interactions, which likely generate the characteristic circular rings and pattern of striations in the outer layer of the bulk φ29 DNA (Fig. 4C), involve contacts at similar or identical locations in most of the gp8 subunits, and hence their arrangement follows the Q=5 head protein lattice. The most prominent

contact seen in the virion reconstruction occurs at one end of the long tubular density on the capsid-interior side of gp8. This feature is modeled, for clarity, as an α-helix in Figure 4b. Lack of an atomic structure of gp8 precludes specific assignment of this DNA-interacting domain. Fitting of an HK97 homology model to the gp8 density (Tang et al., in preparation) suggests that this end of the modeled helix corresponds to the N-terminal end of the HK97 long helix (Wikoff et al., 2000). Whether these regular DNA-shell contacts organize the DNA while it is being packaged or stabilize it in the mature virion has yet to be determined.

Additional views of the connector and its surroundings are revealed in two cross sections made perpendicular to the tail axis, which intersect the top of the connector (Fig. 2B and 2E) and the middle of the lower collar (Fig. 2C and 2F), respectively. A circular ring of density ascribed to DNA and which follows a sinusoidal path in three-dimensions (data not shown) encircles the top of the connector (Fig. 2B). Ring-like DNA structures may be a universal component of dsDNA phages, as they have been observed in ε15 and P22 (Lander et al., 2006; Xiang et al., 2006) as well as ø29 (Jiang et al., 2006), and have also appeared in model simulations of ε15 (Petrov et al., 2007). However, unlike in P22 (Lander et al., 2006), this portion of the ø29 DNA does not appear to contact the connector, but instead appears to be pressed up against the inner wall of the capsid immediately adjacent to the connector. It has been suggested that the DNA ring in P22 controls termination of DNA translocation (Lander et al., 2006). However, ø29 packages a unit length chromosome and does not require such a sensor (Xiang et al., 2006). A ring-like DNA structure may simply arise when portions of the bulk DNA are compressed into the groove between the connector and capsid as simulated in ε15 (Petrov et al., 2007) and hence may have no defined role in packaging in ø29.

In our sub-nanometer reconstruction of the ø29 virion it is possible to identify and trace the path of the right end of the DNA-gp3 molecule, starting from where it emerges from the bulk of the packaged DNA in the head and ending near the distal portion of the tail (Fig 5). Definitive location in virions of the right end of the ø29 DNA and the covalently-attached, gp3 terminal protein is now possible for two primary reasons. We have reconstructions at similar sub-nanometer resolutions of both the empty particle and the full, mature virion. In addition, a column of high density, with a diameter (~20 Å), pitch, and helical morphology characteristic of suitably resolved double-stranded DNA, is visible for the first time in an infectious virus (Fig. 2 and Fig. 5). Indeed, these characteristic features are a consequence of the DNA being similarly oriented and occupying the same location in most phages.

In the virion reconstruction, a cylindrical column of high density emerges from the bulk DNA inside the head, slightly above the connector, and traverses the connector along its axis for ~80 Å (Fig. 2A and Fig. 5). We assign this feature to be DNA rather than protein as was recently suggested (Xiang et al., 2006). Just below the connector-lower collar junction, a second, ~80Å long column of high density traverses the narrow section of the lower collar and continues into the tail tube to a position ~100 Å above the tail knob (Fig. 1B,Fig. 2A, and Fig. 5). The diameter, intensity, and location of this column also led us to identify the density as being dsDNA as well. However, density below and contiguous with this column abruptly weakens in intensity compared to the surrounding tail tube, continues another ~150Å along the tail tube channel and then tapers to a point at the top of the knob cavity formed by gp9 (Fig. 2A and Fig. 6a). We identify this low density feature as belonging to gp3 on the basis of its weaker intensity, its location at the end of the DNA to which it is covalently attached (Meijer et al., 2001), and because it extends over a distance roughly equivalent to the length of an extended gp3 (Kamtekar et al., 2004;Xiang et al., 2006).

The right end of the ϕ29 DNA interacts with portions of the connector, lower collar and tail tube in its path from head to tail (Fig. 6). This segment of the ϕ29 DNA first appears to contact the C-terminus of gp10, where twelve termini form a crown-like structure at the top of the wide

end of the connector. Next, density corresponding to connector channel loops, which are disordered and hence not resolved in the gp10 crystal structure, appear to provide multiple contacts with the DNA, one of which is identified with an arrow in Figure 6A. Similar loops found in the SPP1 phage connector are believed to play a role in DNA translocation (Isidro et al., 2004;Lebedev et al., 2007). In the second column, which lies below the gp10–gp11 junction, the DNA appears to be clamped at the constricted entrance of the tail tube. Finally, the terminal gp3 appears to form a plug that anchors the DNA near the end of the tail tube. The role these DNA-protein interactions play in retaining and subsequently releasing the highly pressurized genome is unknown.

Most notably, the columns of DNA density that traverse the connector and the lower collar in the virion are interrupted by a toroid-like structure in the center of the cavity formed at the connector-lower collar junction (Fig. 2C, 5). The ~20Å thick toroid has outer and inner radii of about 29 and 9 Å, respectively, with no detectable density in its center. The corresponding region in empty particles has no density (Fig. 2F). Based on its dimensions and its close juxtaposition to the high-density columns above and below it that must connect in some way, the toroid appears to represent a novel dsDNA structural motif.

DNA Under Pressure

The DNA toroid is arguably the most intriguing part of the ø29 structure revealed in the virion reconstruction. We questioned whether this feature might arise as an averaging artifact, generated when compressed DNA adopts a consistent (but randomly oriented in different particles) bulge as it passes through the connector-lower collar cavity. However, the doughnut-like morphology, coupled with the observation that the toroid density is comparable in intensity to that in the columns of density above and below it, strongly argues that the toroid is a genuine feature in φ29. The most plausible interpretation of our 3D density map is that, under compression and in the confines of the connector-lower collar cavity, the DNA responds to the high compressive forces exerted upon it (Rickgauer et al., 2008; Smith et al., 2001) by sharply bending into a toroid, with no evidence for extensive contacts with gp10 or gp11 (Fig 5B, 6A).

Detailed inspection and analysis of the virion map showed thinner density features entering and exiting the top and bottom of the toroid, respectively (Fig 3, 5). Apparently, with surprising regularity, the entry and exit points in the toroid occur at the same sites in most virions. Consistent with this, the axis of the toroid is tilted slightly away from the tail axis. If instead the entry and exit points were random, an untilted doughnut would result and little or no density would connect it to the columns of high density above and below it. The well-defined character of the toroid and initial modeling experiments (Tang et a., unpublished) suggest it contains 30 to 40 DNA bases.

Can DNA in fact form such a sharply curved, toroid-like structure? The persistence length of dsDNA is generally reported as ~500Å (Purohit et al., 2005), and hence, energy is required to bend DNA over shorter radii. Though bending required to produce DNA curvature like that predicted for a ~60 Å diameter toroid might seem extreme, it has recently been noted that "Tightly bent DNA is a fact of life" (Garcia et al., 2007). It is also known that, in the presence of DNA-binding proteins such as integration host factor (IHF) (Rice et al., 1996), DNA can be bent as tightly as seen here in ø29.

The toroid structure we observe in φ29 appears to represent a novel mode of DNA bending, possibly driven by compression of the DNA in a confined volume. During packaging, a force of ~100 pN is required to insert the last of the DNA into the head (Rickgauer et al., 2008). Even if some of this stored energy dissipates after packaging is complete, the DNA molecule remains under significant tension (Gonzalez-Huici et al., 2004; Purohit et al., 2005). To our knowledge, no experimental system has probed how dsDNA responds to compression when

it is tightly constrained such as in the confines of the ø29 phage tail. Under high compression and bounded by the connector-collar cavity, the DNA might behave like a stiff, yet flexible string, that tends to naturally fold into a toroid when two fixed points on it are brought together. What role, if any, the ϕ29 DNA toroid serves remains a mystery. This structure might assist in holding the pressurized DNA in the tail while it awaits ejection during infection. Analysis of the toroid by cryoEM at higher resolution, coupled with demonstration of its presence in other phages, will help determine if the toroid is a key factor in making ϕ29 and counterparts such efficient and precise DNA-delivery machines.

EXPERIMENTAL PROCEDURES

Fiberless ø29 virions and empty particles were prepared and purified as previously described for fibered phage (Tao et al., 1998). Briefly, empty particles were made by incubating virions in 1 M sodium perchlorate in TMS buffer for 16 hr at 37°C, followed by repurification by isopycnic centrifugation in CsCl. Samples of ø29 were vitrified over holey, carbon-coated grids and imaged at 200 keV and at a nominal magnification of 38,000X on Kodak SO163 electron image film at low electron doses (~20e-/Å^2) in an FEI CM200 FEG microscope. Micrographs exhibiting minimal astigmatism and specimen drift and under-focused 1–5 µm were digitized at 7 µm intervals on a Zeiss PHODIS scanner and bin averaged to yield an effective pixel size of 3.68 Å. A total of 74 and 122 micrographs of the full and empty particles, respectively, were selected for particle boxing using the program RobEM (http://cryoem.ucsd.edu/programs.shtml).

Asymmetric 3D reconstructions of the fiberless ϕ29 particles were computed using a modified, model-based scheme (Baker and Cheng, 1996; Baker et al., 1999; Ji et al., 2006). First, we used EMAN (Ludtke et al., 2004) and a ϕ29 prohead reconstruction (Morais et al., 2005) to generate a five-fold symmetric reconstruction of the fiberless ϕ29 capsid. Several cycles of refinement, with images repeatedly remasked to include progressively more of the tail in each image, led to a hybrid model, with five- and twelve-fold symmetrized head and tail components, respectively. We then used this model in EMAN to produce an asymmetric reconstruction of the fiberless virion at about 30-Å resolution. With this reconstruction, we next used FREALIGN (Grigorieff, 2007) to assign origin and orientation parameters to each image and to produce an asymmetric phage reconstruction at ~25-Å resolution. This then served as the starting model for extensive, iterative refinement at higher resolution using modified versions of our parallelized origin and orientation refinement program, POOR (Ji et al., 2006) and parallelized 3D reconstruction program, P3DR (Marinescu and Ji, 2003). Both of these programs were implemented without any symmetry constraints being imposed, and yielded a 3D map of the virion from 12682 particle images at a resolution estimated to be reliable to 7.8 Å, using Fourier Shell Correlation criteria (Van Heel and Harauz, 1986)(0.5 threshold). The protocol outlined above was similarly used to produce a 9.3 Å resolution map of the fiberless ϕ29 empty particle from 12829 particle images.

For visualization purposes, a segmentation program (Yu and Bajaj, 2005) was used to help delineate the ϕ29 DNA in the virion 3D map. The molecular envelopes of the protein components were estimated manually in CHIMERA (Goddard et al., 2005) as guided by existing knowledge of ϕ29 (Grimes et al., 2002). However, the precise delineations of these envelopes, especially at intersubunit boundaries, are not known.

The atomic model of the gp10 dodecamer crystal structure (PDB Accession code 1H5W) was manually fitted and subsequently computationally adjusted to best fit the cryoEM density maps with a modified version of RSREF (Tang et al., 2001). Illustrations were composed using the CHIMERA (Goddard et al., 2005) and RobEM (http://cryoem.ucsd.edu/programs.shtml) programs.

ACKNOWLEDGEMENTS

REFERENCES

Aebi U, Bijlenga R, v d Broek J, v d Broek H, Eiserling F, Kellenberger C, Kellenberger E, Mesyanzhinov V, Muller L, Showe M, et al. The transformation of tau particles into T4 heads. II. Transformations of the surface lattice and related observations on form determination. J. Supramol. Struct 1974;2:253–275. [PubMed: 4612249]

Agirrezabala X, Martín-Benito J, Castón JR, Miranda R, Valpuesta JM, Carrascosa JL. Maturation of phage T7 involves structural modification of both shell and inner core components. Embo J 2005;24:3820–3829. [PubMed: 16211007]

Allen GS, Frank J. Structural insights on the translation initiation complex: ghosts of a universal initiation complex. Mol. Microbiol 2007;63:941–950. [PubMed: 17238926]

Anderson, D.; Reilly, B. Bacteriophage □29 morphogenesis. In: Hoch, JA.; Losick, R.; Sonenshein, AL., editors. *Bacillus subtilis* and Other Gram Positive Bacteria: Physiology, Biochemistry, and Molecular Genetics. Washington, D.C.: ASM Publications; 1993. p. 859-867.

Baker ML, Jiang W, Rixon FJ, Chiu W. Common ancestry of herpesviruses and tailed DNA bacteriophages. J. Virol 2005;79:14967–14970. [PubMed: 16282496]

Baker TS, Cheng RH. A model-based approach for determining orientations of biological macromolecules imaged by cryoelectron microscopy. J. Struct. Biol 1996;116:120–130. [PubMed: 8742733]

Baker TS, Olson NH, Fuller SD. Adding the third dimension to virus life cycles: three-dimensional reconstruction of icosahedral viruses from cryo-electron micrographs. Microbiol. Mol. Biol. Rev 1999;63:862–922. [PubMed: 10585969]

Berk V, Cate JH. Insights into protein biosynthesis from structures of bacterial ribosomes. Curr. Opin. Struct. Biol 2007;17:302–309. [PubMed: 17574829]

Bottcher B, Wynne SA, Crowther RA. Determination of the fold of the core protein of hepatitis B virus by electron cryomicroscopy. Nature 1997;386:86–91.

Carrascosa JL, Carazo JM, Garcia N. Structural localization of the proteins of the head to tail connecting region of bacteriophage φ29. Virology 1983;124:133–143.

Chang J, Weigele P, King J, Chiu W, Jiang W. Cryo-EM asymmetric reconstruction of bacteriophage P22 reveals organization of its DNA packaging and infecting machinery. Structure 2006;14:1073–1082. [PubMed: 16730179]

Chemla YR, Aathavan K, Michaelis J, Grimes S, Jardine PJ, Anderson DL, Bustamante C. Mechanism of force generation of a viral DNA packaging motor. Cell 2005;122:683–692. [PubMed: 16143101]

Comolli LR, Spakowitzb AJ, Siegeristc CE, Jardine PJ, Grimes S, Anderson DL, Bustamante C, Downing KH. Three-dimensional architecture of the bacteriophage φ29 packaged genome and elucidation of its packaging process. Virology. 2007in press

Conway JF, Cheng N, Zlotnick A, Wingfield PT, Stahl SJ, Steven AC. Visualization of a 4-helix bundle in the hepatitis B virus capsid by cryo-electron microscopy. Nature 1997;386:91–94. [PubMed: 9052787]

Garcia HG, Grayson P, Han L, Inamdar M, Kondev J, Nelson PC, Phillips R, Widom J, Wiggins PA. Biological consequences of tightly bent DNA: the other life of a macromolecular celebrity. Biopolymers 2007;85:115–130. [PubMed: 17103419]

Goddard TD, Huang CC, Ferrin TE. Software extensions to UCSF chimera for interactive visualization of large molecular assemblies. Structure 2005;13:473–482. [PubMed: 15766548]

Gonzalez-Huici V, Salas M, Hermoso JM. The push-pull mechanism of bacteriophage φ29 DNA injection. Mol. Microbiol 2004;52:529–540. [PubMed: 15066038]

Grigorieff N. FREALIGN: high-resolution refinement of single particle structures. J. Struct. Biol 2007;157:117–125. [PubMed: 16828314]

Grimes S, Jardine PJ, Anderson D. Bacteriophage φ29 DNA packaging. Adv. Virus Res 2002;58:255–294. [PubMed: 12205781]

Guasch A, Pous J, Ibarra B, Gomis-Ruth FX, Valpuesta JM, Sousa N, Carrascosa JL, Coll M. Detailed architecture of a DNA translocating machine: the high-resolution structure of the bacteriophage φ29 connector particle. J. Mol. Biol 2002;315:663–676. [PubMed: 11812138]

Hagen EW, Reilly BE, Tosi ME, Anderson DL. Analysis of gene function of bacteriophage φ29 of *Bacillus subtilis*: identification of cistrons essential for viral assembly. J. Virol 1976;19:501–517. [PubMed: 822175]

Hendrix RW. Symmetry mismatch and DNA packaging in large bacteriophages. Proc. Nat'l. Acad. Sci. USA 1978;75:4779–4783. [PubMed: 283391]

Isidro A, Santos MA, Henriques AO, Tavares P. The high-resolution functional map of bacteriophage SPP1 portal protein. Mol. Microbiol 2004;51:949–962. [PubMed: 14763972]

Jäälinoja HT, Huiskonen JT, Butcher SJ. Electron cryomicroscopy comparison of the architectures of the enveloped bacteriophages Φ6 and Φ8. Structure 2007;15:157–167. [PubMed: 17292834]

Ji Y, Marinescu DC, Zhang W, Zhang X, Yan X, Baker TS. A model-based parallel origin and orientation refinement algorithm for cryoTEM and its application to the study of virus structures. J. Struct. Biol 2006;154:1–19. [PubMed: 16459100]

Jiang W, Chang J, Jakana J, Weigele P, King J, Chiu W. Structure of epsilon15 bacteriophage reveals genome organization and DNA packaging/injection apparatus. Nature 2006;439:612–616. [PubMed: 16452981]

Jiang W, Ludtke SJ. Electron cryomicroscopy of single particles at subnanometer resolution. Cur. Opin. Struct. Biol 2005;15:571–577.

Johnson JE, Chiu W. DNA packaging and delivery machines in tailed bacteriophages. Curr. Opin. Struct. Biol 2007;17:237–243. [PubMed: 17395453]

Kamtekar S, Berman AJ, Wang J, Lazaro JM, de Vega M, Blanco L, Salas M, Steitz TA. Insights into strand displacement and processivity from the crystal structure of the protein-primed DNA polymerase of bacteriophage Φ29. Mol. Cell 2004;16:609–618. [PubMed: 15546620]

Lander GC, Tang L, Casjens SR, Gilcrease EB, Prevelige P, Poliakov A, Potter CS, Carragher B, Johnson JE. The structure of an infectious P22 virion shows the signal for headful DNA packaging. Science 2006;312:1791–1795. [PubMed: 16709746]

Lebedev AA, Krause MH, Isidro AL, Vagin AA, Orlova EV, Turner J, Dodson EJ, Tavares P, Antson AA. Structural framework for DNA translocation via the viral portal protein. Embo J 2007;26:1984–1994. [PubMed: 17363899]

Ludtke SJ, Chen DH, Song JL, Chuang DT, Chiu W. Seeing GroEL at 6 Å resolution by single particle electron cryomicroscopy. Structure 2004;12:1129–1136. [PubMed: 15242589]

Marinescu DC, Ji Y. A computational framework for the 3D structure determination of viruses with unknown symmetry. J. Parallel Distrib. Comput 2003;63:738–758.

Meijer WJ, Horcajadas JA, Salas M. Phi29 family of phages. Microbiol. Mol. Biol. Rev 2001;65:261–287. [PubMed: 11381102]

Mitra K, Frank J. Ribosome dynamics: insights from atomic structure modeling into cryo-electron microscopy maps. Ann.Rev. Biophys. Biomol. Struct 2006;35:299–317. [PubMed: 16689638]

Morais MC, Choi KH, Koti JS, Chipman PR, Anderson DL, Rossmann MG. Conservation of the capsid structure in tailed dsDNA bacteriophages: the pseudoatomic structure of φ29. Mol. Cell 2005;18:149–159. [PubMed: 15837419]

Morais MC, Kanamaru S, Badasso MO, Koti JS, Owen BA, McMurray CT, Anderson DL, Rossmann MG. Bacteriophage φ29 scaffolding protein gp7 before and after prohead assembly. Nat. Struct. Biol 2003;10:572–576. [PubMed: 12778115]

Morais MC, Tao Y, Olson NH, Grimes S, Jardine PJ, Anderson DL, Baker TS, Rossmann MG. Cryoelectron-microscopy image reconstruction of symmetry mismatches in bacteriophage φ29. J. Struct. Biol 2001;135:38–46. [PubMed: 11562164]

Peterson C, Simon M, Hodges J, Mertens P, Higgins L, Egelman E, Anderson D. Composition and mass of the bacteriophage φ29 prohead and virion. J. Struct. Biol 2001;135:18–25. [PubMed: 11562162]

Petrov AS, Harvey SC. Structural and thermodynamic principles of viral packaging. Structure 2007;15:21–27. [PubMed: 17223529]

Petrov AS, Lim-Hing K, Harvey SC. Packaging of DNA by bacteriophage ε15: structure, forces, and thermodynamics. Structure 2007;15:807–812. [PubMed: 17637341]

Purohit PK, Inamdar MM, Grayson PD, Squires TM, Kondev J, Phillips R. Forces during bacteriophage DNA packaging and ejection. Biophys. J 2005;88:851–866. [PubMed: 15556983]

Rice PA, Yang S, Mizuuchi K, Nash HA. Crystal structure of an IHF-DNA complex: a protein-induced DNA U-turn. Cell 1996;87:1295–1306. [PubMed: 8980235]

Rickgauer JP, Fuller DN, Grimes S, Jardine PJ, Anderson DL, Smith DE. Portal motor velocity and capsid pressure during viral DNA packaging in bacteriophage φ29. Biophys. J 2008;94:159–167. [PubMed: 17827233]

Simpson AA, Tao Y, Leiman PG, Badasso MO, He Y, Jardine PJ, Olson NH, Morais MC, Grimes S, Anderson DL, et al. Structure of the bacteriophage φ29 DNA packaging motor. Nature 2000;408:745–750. [PubMed: 11130079]

Smith DE, Tans SJ, Smith SB, Grimes S, Anderson DL, Bustamante C. The bacteriophage straight Φ29 portal motor can package DNA against a large internal force. Nature 2001;413:748–752. [PubMed: 11607035]

Subirana JA, Lloveras J, Lombardero M, Vinuela E. X-ray scattering of the non-isometric *Bacillus subtilis* phage φ29. J. Mol. Biol 1979;128:101–106. [PubMed: 107319]

Tang J, Taylor DW, Taylor KA. The three-dimensional structure of alpha-actinin obtained by cryoelectron microscopy suggests a model for Ca(2+)-dependent actin binding. J. Mol. Biol 2001;310:845–858. [PubMed: 11453692]

Tao Y, Olson NH, Xu W, Anderson DL, Rossmann MG, Baker TS. Assembly of a tailed bacterial virus and its genome release studied in three dimensions. Cell 1998;95:431–437. [PubMed: 9814712]

Trus BL, Roden RB, Greenstone HL, Vrhel M, Schiller JT, Booy FP. Novel structural features of bovine papillomavirus capsid revealed by a three-dimensional reconstruction to 9 Å resolution. Nat. Struct. Biol 1997;4:413–420. [PubMed: 9145113]

Van Heel M, Harauz G. Resolution criteria for three dimensional reconstruction. Optik 1986;73:119–122.

Wikoff WR, Liljas L, Duda RL, Tsuruta H, Hendrix RW, Johnson JE. Topologically linked protein rings in the bacteriophage HK97 capsid. Science 2000;289:2129–2133. [PubMed: 11000116]

Xiang Y, Morais MC, Battisti AJ, Grimes S, Jardine PJ, Anderson DL, Rossmann MG. Structural changes of bacteriophage φ29 upon DNA packaging and release. Embo J 2006;25:5229–5239. [PubMed: 17053784]

Yu Z, Bajaj C. Automatic ultrastructure segmentation of reconstructed cryoEM maps of icosahedral viruses. IEEE Trans. Image Process 2005;14:1324–1337. [PubMed: 16190468]

Zhang X, Ji Y, Zhang L, Harrison SC, Marinescu DC, Nibert ML, Baker TS. Features of reovirus outer capsid protein µ1 revealed by electron cryomicroscopy and image reconstruction of the virion at 7.0 Å resolution. Structure 2005;13:1545–1557. [PubMed: 16216585]

Zhou ZH, Baker ML, Jiang W, Dougherty M, Jakana J, Dong G, Lu G, Chiu W. Electron cryomicroscopy and bioinformatics suggest protein fold models for rice dwarf virus. Nat. Struct. Biol 2001;8:868–873. [PubMed: 11573092]
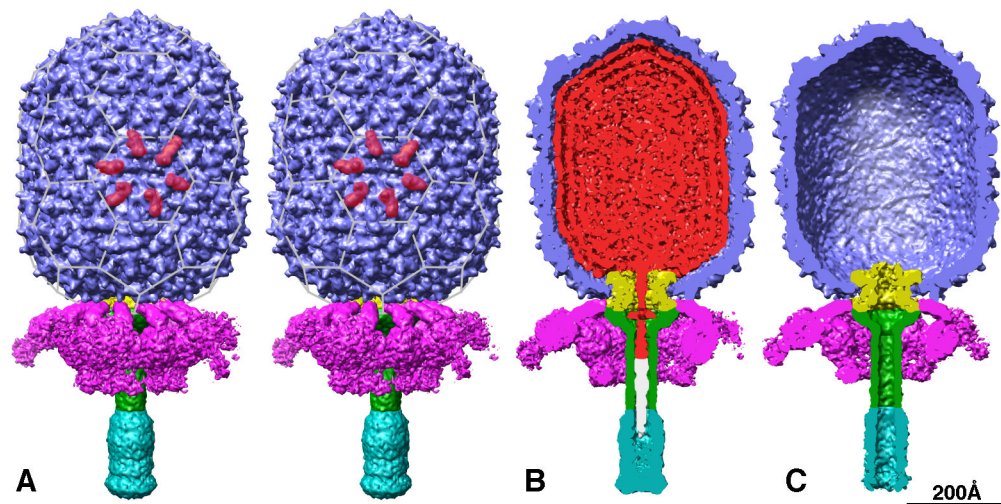
Fig 1.
Solid-surface representations of the fiberless ϕ29 virion and empty particle 3D reconstructions, segmented and color-coded to highlight different components. (A) Stereo view of the virion with a Q=5 lattice (gray) added to highlight the arrangement of pentameric and hexameric capsomeres in the prolate head. The BIG2 protrusion domains in one hexamer of gp8 are highlighted in red. (B) Monoscopic view of virion with front half removed to show interior components. (C) Same as (b) for empty particle. Color scheme: capsid (gp8) - blue; connector (gp10) – yellow; lower collar and tube (gp11) – green; knob (gp9) – cyan; appendages (gp12*) – magenta; terminal protein (gp3) on right end of DNA – white; and DNA alone - red. Density threshold (~1σ) yields the expected volume of the components.
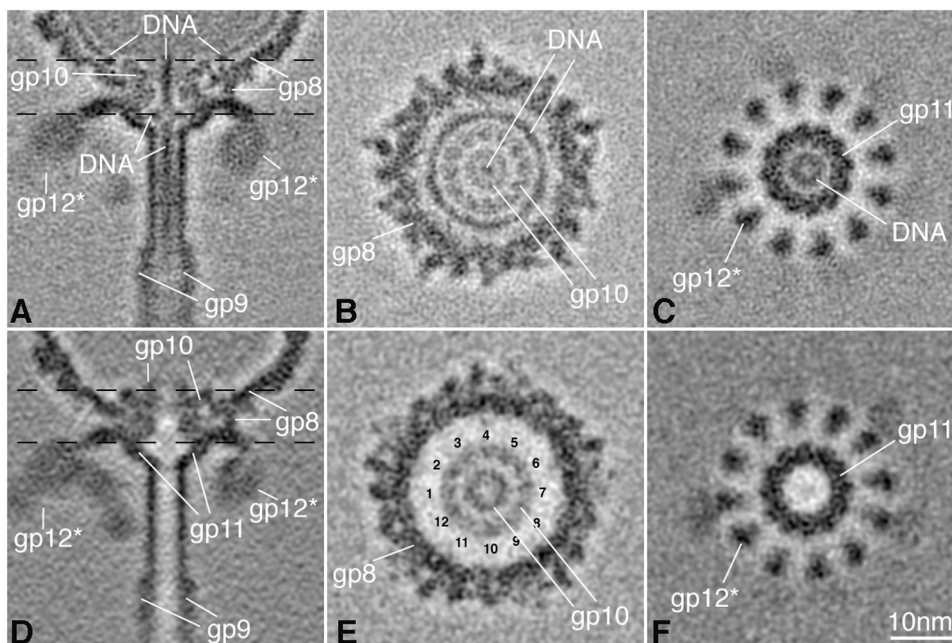
Fig 2.
Density sections from the tail regions in the fiberless φ29 full (A–C) and empty (D–F) particles. Features with highest or lowest densities appear darkest and lightest, respectively. (A) Longitudinal section of the virion reconstruction labeled to highlight the locations of some phage components. (B,C) Density sections normal to the tail axis at the locations depicted by dashed lines in (A) intersect two portions of the top of the gp10 connector in (B) and the middle of the gp11 lower collar in (C). (D–F) Same as (A–C) for the empty particle. The predominant density features, seen in the virion but not in the empty particle reconstructions, are identified as belonging to DNA and gp3. These include i) the ring of ~190Å diameter that encircles the gp10 dodecamer inside the capsid (B), ii) linear columns positioned along the phage axis and traversing the connector (A,B) and upper tail tube (A), iii) the ~60Å diameter toroid in the connector-collar cavity (A,C), and iv) more diffuse density in the lower portion of the tail tube, terminating at the entrance to the tail knob cavity (A). The twelve asymmetrically arranged copies of gp10 are labeled in (E) but not (B). Scale bar in (F) applies to all panels.
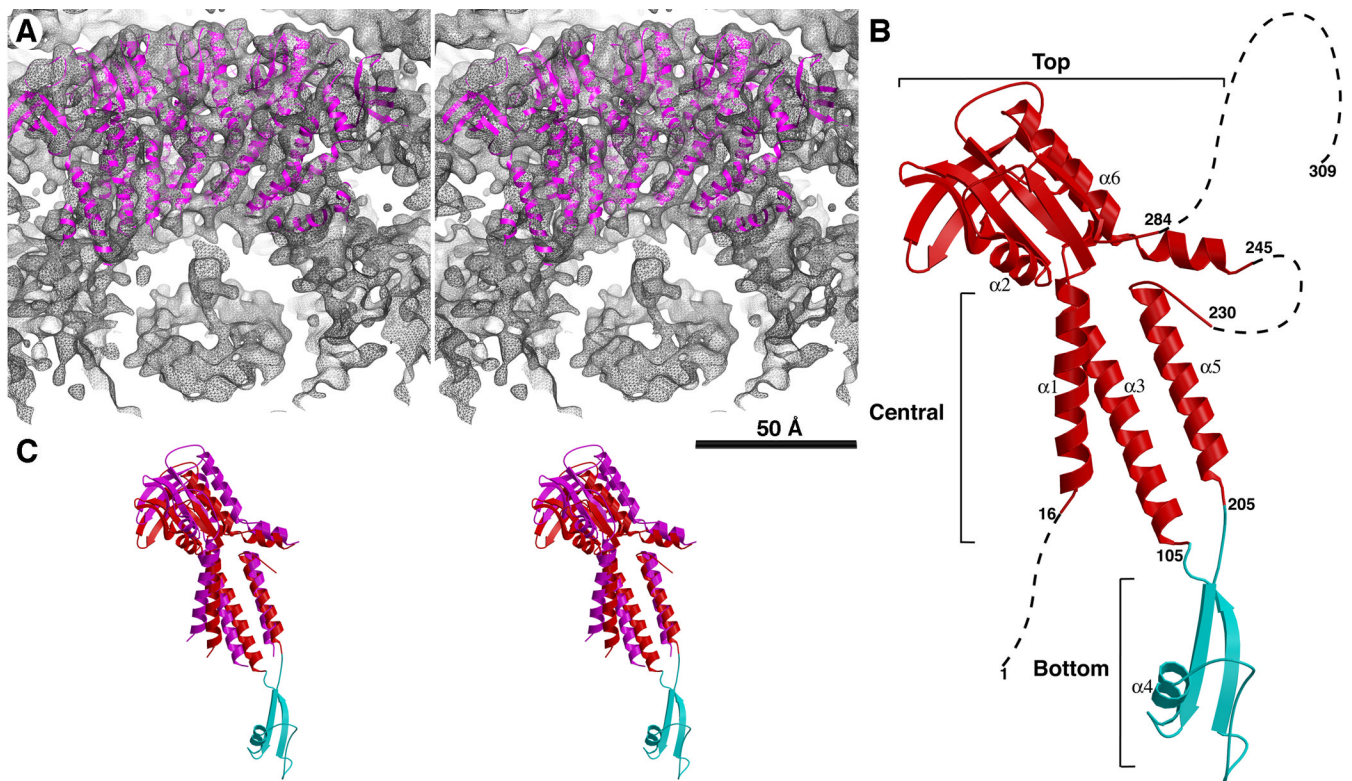
Fig 3.
Connector structure in the fiberless ϕ29 virion and in crystals. (A) Stereo view of a portion of the connector region in the reconstructed virion density map (gray wire mesh; ~2σ threshold) into which an atomic model (magenta ribbon diagram) of the X-ray crystal structure of the connector (Guasch et al., 2002) was docked. The gp10 subunits of the model were adjusted, essentially as a set of rigid bodies, to best fit the prominent α-helices into the corresponding tubes of density in the reconstructed 3D map. (B) Tertiary structure of the gp10 monomer in crystals of the symmetric dodecamer (Guasch et al., 2002). Top and central (in red), and bottom (cyan) domains in gp10 are identified. Highly flexible regions, invisible in the gp10 X-ray structure are indicated by dashed curves. Helices (α1–α6) are labeled according to their location in the primary amino acid sequence (α6 is kinked, with short and long segments). (C) Stereo view showing a ribbon diagram of the gp10 crystal structure (red and cyan) superimposed with a fitted virion model (magenta). The bottom domain (B) was not modeled in the virion density map (see text).
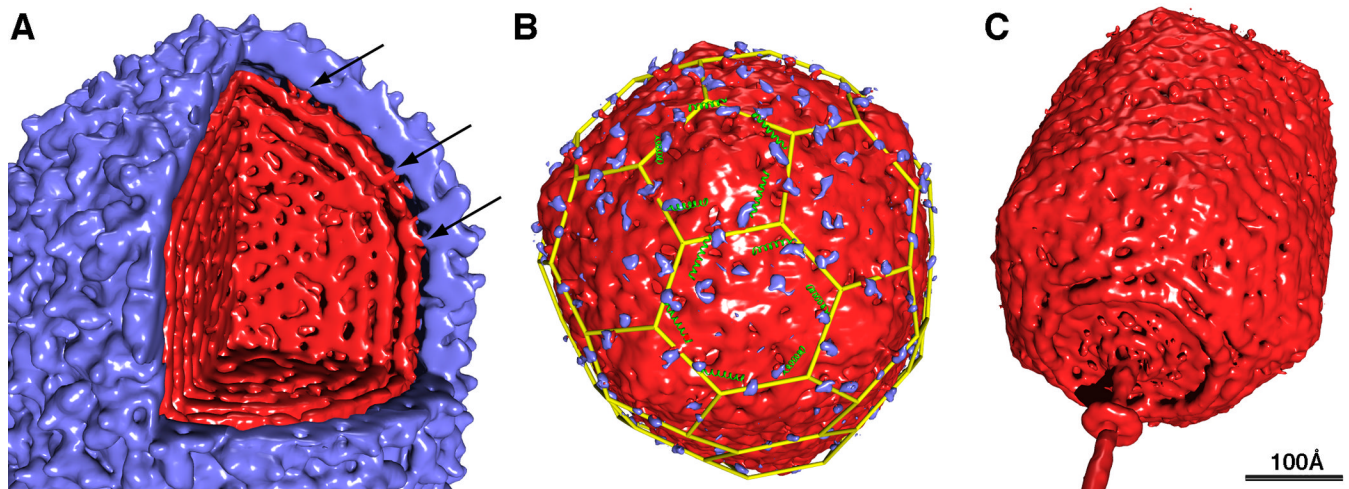
Fig 4.
DNA organization in φ29. (A) Cutaway view of the φ29 virion head, showing the compact layers in the bulk DNA (red). Four layers are clearly visible, with the outermost one closely following and interacting with the capsid (blue) inner surface in several places (e.g. arrows). (B) Near axial view of the virion, looking towards the tail with most of the capsid density removed. This highlights numerous contacts between the capsid and bulk DNA. These contacts, which are colored blue but may include protein, DNA or a mixture, predominantly occur near the same end of the long α-helix in each gp8 (green helical ribbons) and cluster near the Q=5 lattice edges (yellow lines). (C) Structure of DNA, segmented from the mature phage (Fig. 1B), viewed from below the tail towards the top of the head. The outermost layer of the bulk DNA contains numerous latitudinal striations as well as a ring of density that encircles but does not contact the connector at the base of the head. Two linear columns of density, each ~20Å in diameter, and the ~60Å diameter toroid sandwiched between them lie along the tail axis. Density thresholds set to ~1σ (panels A and B) and ~2σ (panel C). The higher threshold in (C) was chosen to emphasize the DNA packing.
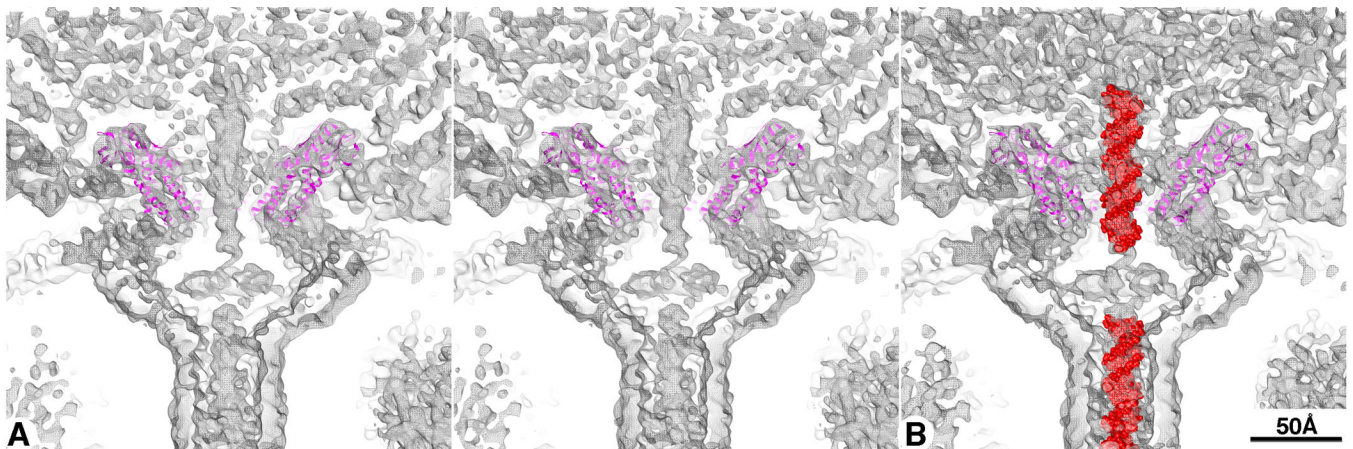
Fig 5.
DNA structure in tail of ϕ29 virion. (A) Stereo view of the reconstructed virion density map (gray wire mesh; ~2σ threshold) in the region near the tail into which a model (magenta ribbon diagram) of the gp10 structure (Guasch et al., 2002) was fitted. Two columns of density, along the tail axis, lie above and below a doughnut-shaped feature centered in the cavity formed by gp10 and gp11. The density threshold of the map was raised to help emphasize boundaries between viral components. (B) Monoscopic view at lower density threshold than used in (A) shows two segments of linear, dsDNA atomic models (space-filling representation), placed into the columns of density. These models do not represent accurate, fitted structures but they do illustrate that the density features are consistent with the size and dimensions of dsDNA.
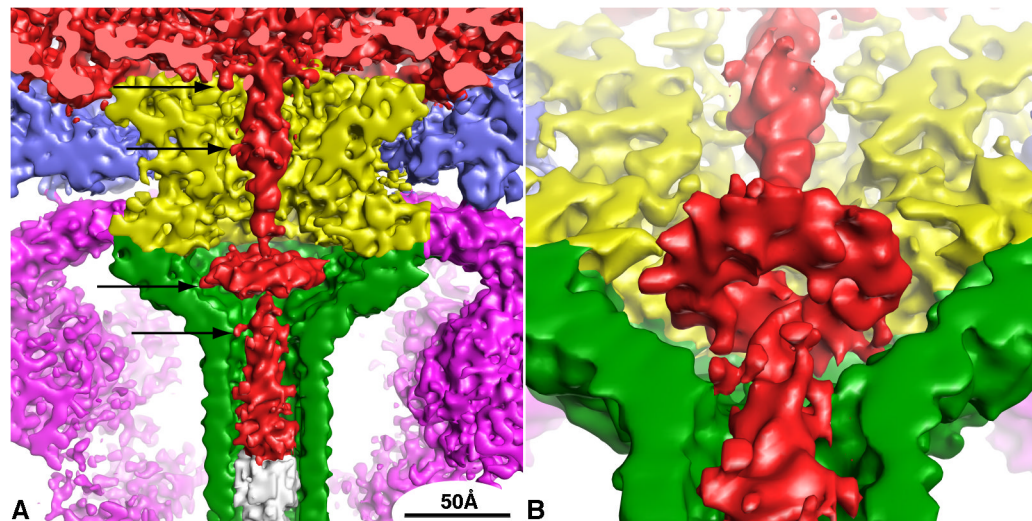
Fig 6.
DNA path through the connector, lower collar, and tail tube viewed in segmented representations of the ϕ29 virion density map (~2σ threshold). (A) A cylindrical column of high density emerges from the bulk DNA (red) in the head, slightly above the connector (yellow), and follows a path along the connector-tail axis into the gp10/11 cavity where it transforms into a toroid-shaped structure. From there, a column of high density emerges at the bottom of the toroid, continues for ~80 Å along the tail tube axis, after which weaker density (white) fills the rest of the tube, ending at the gp9 tail knob cavity (not shown). Four arrows identify regions in the plane of the cross section where the DNA and gp10 (yellow) and gp11 (green) are in close contact. These contacts, along with the apparent tight interactions between the DNA-gp3 and the end of the tail tube, might collectively help prime the highly pressurized DNA for release upon attachment of the phage to the host. (B) Tilted, close-up view of the DNA toroid and its surroundings. Color scheme matches that used in Figure 1.